COBEM UBERLÂNDIA 2019

ABCM
25th ABCM International Congress of Mechanical Engineering
October 20-25, 2019, Uberlândia, MG, Brazil

A STUDY ON THE EFFECTS OF OBSTACLES ON THE FLOW IN A VENTILATED CAVITY

Marlon de Novaes Batista Filho
Adriano Possebon Rosa
Vortex (Laboratory of Microhydrodynamics and Rheology) - Department of Mechanical Engineering - University of Brasília
mecanicamnbf@gmail.com
aprosa@unb.br

Abstract. *In this work we investigate numerically the influence of square obstacles on the flow of an incompressible Newtonian fluid inside a two-dimensional ventilated cavity. Our objective is to analyze the flow configurations and to examine the changes in the pressure drop between the inlet and the outlet ports as a function of the size of the obstacles, their position inside the cavity and of the Reynolds number. For this purpose, we use a second order projection method coupled with a finite difference discretization scheme to evolve the Navier-Stokes equations and to keep the velocity field solenoidal. The flow in a ventilated cavity is important in many technical applications, such as microelectronic cooling and in the process of ventilation inside buildings.*

Keywords: *Ventilated Cavity, Obstacle, Projection Method, Pressure Drop*

1. INTRODUCTION

The flow in a closed cavity generated by a moving solid boundary is a classical problem in the field of computer fluid mechanics and is of large importance for many industrial applications (Shankar and Deshpande, 2000; Erturk, 2009). This flow is also used to validate and test numerical codes. Another important situation of fluid flow is the one characterized by a ventilated cavity with an inlet and an outlet port (Saeidi and Khodadadi, 2006). This ventilated cavity associated with the presence of internal solid obstacles has many applications, as in the cooling of electronic components, in the ventilation of buildings (Limane *et al.*, 2015) and in the design of solar collectors (Mushatet, 2011). The presence of obstacles close to the walls is also shown to enhance the mixing process in the flow inside a cavity (Maneshian *et al.*, 2019).

Over the past years, the flow in a ventilated cavity and the flow in closed environments in the presence of obstacles have received great attention. The patterns of the flow can affect the pressure drop between the entrance and the exit of the domain and may also affect the heat exchange between the obstacle and the fluid. Korichi and Oufer (2007) investigated the possibility of heat transfer enhancement on the flow between two parallel plates with alternated obstacles attached to the walls. The authors investigated flows with Reynolds numbers between 50 and 1000. One of their conclusions is that arranging the obstacles on both walls can increase significantly the flow-obstacle heat exchange. Saeidi and Khodadadi (2006) investigated the flow in a ventilated cavity with the walls at a lower temperature than the incoming fluid. They examined different positions and sizes for the inlet and outlet ports. The analysis was based on the flow configurations, on the pressure drop and on the resulting Nusselt number. Madadi and Balaji (2008) used neural networks to analyze the optimum position placement, inside a ventilated cavity, of three obstacles that are also heat sources.

At the same time, the behavior of complex fluids in similar flows have also been analyzed by many authors. Sourtiji *et al.* (2014), for example, investigated the behavior of a suspension of aluminum oxide in water in a ventilated cavity, while the flow of a ferrofluid in a ventilated cavity with a circular rotating obstacle was analyzed by Selimefendigil and Oztop (2014).

In the present paper, we simulate numerically the flow in a two-dimensional ventilated cavity with obstacles of different sizes and placed in different positions. The fluid is taken as a Newtonian incompressible one and a finite difference scheme coupled with a second order projection method is used. The main goal here is to analyze the effects of the obstacles and the Reynolds number on the pressure drop between the inlet and the outlet ports and on the flow configurations.

2. GOVERNING EQUATIONS AND FLOW DETAILS

The geometry of the problem under investigation in this work is outlined in Fig. 1. The size of the square cavity is L, and the inlet and outlet port widths are L_{in} and L_{out}, respectively. A solid obstacle, of size L_{obs}, is also shown in Fig. 1. Finally, U_{in} represents the average velocity with which the fluid enters the cavity.

The governing equations are the mass conservation equation for an incompressible fluid,

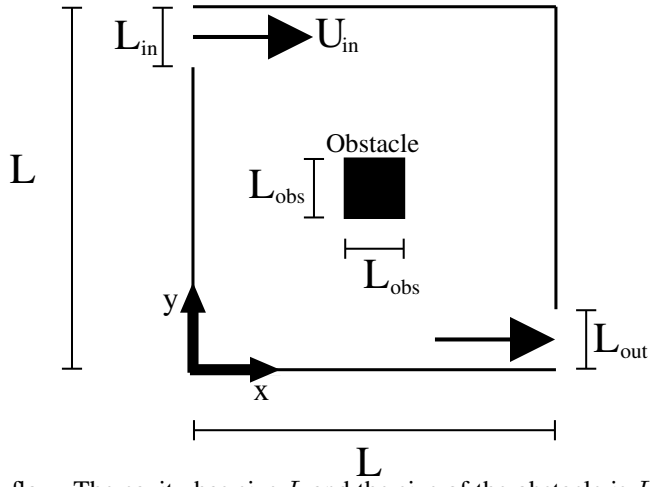

Figure 1: Geometry of the flow. The cavity has size L and the size of the obstacle is L_{obs}. The average inlet velocity is U_{in} and the widths of the inlet and outlet ports are L_{in} and L_{out}, respectively.

$$\boldsymbol{\nabla} \cdot \boldsymbol{u} = 0 \ , \tag{1}$$

and the momentum equation,

$$\frac{\partial \boldsymbol{u}}{\partial t} + \boldsymbol{u} \cdot \boldsymbol{\nabla} \boldsymbol{u} = -\boldsymbol{\nabla} p + \frac{1}{Re} \nabla^2 \boldsymbol{u} \ . \tag{2}$$

Here, $\boldsymbol{\nabla} = \hat{\boldsymbol{e}}_x \partial/\partial x + \hat{\boldsymbol{e}}_y \partial/\partial y$ is the nabla operator, $\boldsymbol{u} = u(x,y)\hat{\boldsymbol{e}}_x + v(x,y)\hat{\boldsymbol{e}}_y$ is a two-dimensional velocity field, t represents the time and p is the pressure. Equations (1) and (2) are in a non-dimensional form, with the size L of the cavity and U_{in} being the characteristic parameters. The Reynolds number in Eq. (2) is defined as

$$Re = \frac{\rho U_{in} L}{\mu} \ , \tag{3}$$

where ρ is the density of the fluid and μ represents its dynamic viscosity.

3. NUMERICAL IMPLEMENTATION

In order to solve Eqs. (1) and (2), we use the projection method (Chorin, 1968; Temam, 1969). In this work, specifically, a second order algorithm proposed by Bell *et al.* (1989) and modified by Brown *et al.* (2001) is employed. The method consists, initially, in the calculation of an intermediary velocity field $\boldsymbol{u}^*$ that does not necessarily represents an incompressible flow. In the following step, this intermediary velocity field is adjusted with a pressure-like function ϕ and projected into a divergence-free vector space. The method is described in the following paragraphs.

First, the velocity $\boldsymbol{u}^*$ is obtained by

$$\frac{\boldsymbol{u}^* - \boldsymbol{u}^k}{\Delta t} + \left(\boldsymbol{u}^{k+1/2} \cdot \nabla\right) \boldsymbol{u}^{k+1/2} = \frac{1}{2Re} \nabla^2 \left(\boldsymbol{u}^* + \boldsymbol{u}^k\right) - \nabla p^{k-1/2} \ . \tag{4}$$

Then, the pressure-like function ϕ is computed

$$\nabla^2 \phi^{k+1} = \frac{1}{\Delta t} \boldsymbol{\nabla} \cdot \boldsymbol{u}^* \ . \tag{5}$$

Finally, the new velocity and the new pressure are calculated, respectively, as

$$\boldsymbol{u}^{k+1} = \boldsymbol{u}^* - \Delta t \boldsymbol{\nabla} \phi^{k+1} \tag{6}$$

and

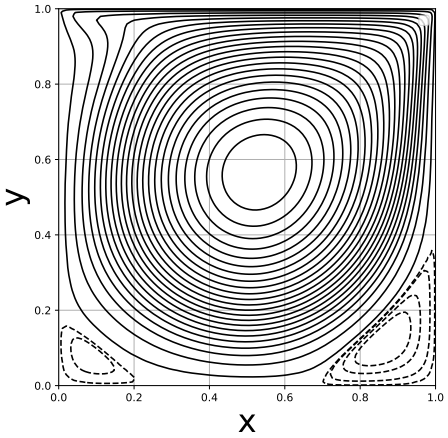

Figure 2: Simulation of a closed cavity with the upper boundary moving to the right, for $Re = 1000$.

Table 1: Maximum value of the stream function. * In this case the Re number was 0.01.

Re	This work	Kim and Moin (1985)	Ghia *et al.* (1982)	Marchi *et al.* (2009)
1	0.0998	0.099	-	0.10008 *
100	0.1033	0.103	0.103	0.10352
400	0.1139	0.112	0.114	0.11399
1000	0.1190	0.116	0.118	0.11894

$$p^{k+1/2} = p^{k-1/2} + \phi^{k+1} - \frac{\Delta t}{2Re}\nabla^2\phi^{k+1} \ . \tag{7}$$

In the above equations, Δt is the numerical time step and $\boldsymbol{u}^k$ approximates the true solution $\boldsymbol{u}$ in time $t = k\Delta t$. Note that the pressure is given in an intermediate time between two subsequent simulation steps. The spatial derivatives are calculated by a standard second order finite difference scheme and it was used a uniform staggered grid for the domain discretization. For the convective terms, we used a second order upwind approximation.

The boundary conditions are imposed over $\boldsymbol{u}^*$ and ϕ. For solid walls, we impose that $\boldsymbol{u}^*$ has the velocity of the wall and also that $\partial\phi/\partial n = 0$, where n represents the normal direction to the wall. For the ventilated cavity, the velocity is defined in the entrance and $\partial\phi/\partial n = 0$. At the exit, $\phi = 0$ and $\partial u/\partial n = \partial v/\partial n = 0$.

3.1 Validation

Before the discussions about the main results, we present in this section a brief validation of the implemented numerical code. First, we simulated the classical problem of a square closed cavity with the upper boundary in constant and uniform motion. In this situation, the Reynolds number is defined as $Re = \rho U L/\mu$, where U is the velocity of the top wall. The plot in Fig. 2 shows some contour lines for the stream function Ψ for $Re = 1000$. It was used, for these simulations, 100 points in the grid in each direction. Also, $\Delta t = 0.005$ and the plot represents a permanent situation. This result agrees, qualitatively, with the plots shown by Botella and Peyret (1998) and Erturk (2009). Table 1 shows some results for the maximum values of the stream function Ψ inside the cavity, for different Re. There is a good agreement between the present results and the results of the references shown in Tab. 1. Figures 3a and 3b show the comparison between the u-velocity profile for $Re = 100$ and $Re = 1000$, respectively, with good agreement when compared to the profiles obtained by Ghia *et al.* (1982).

After the implementation and validation of the code in a closed cavity, the next step was to introduce the fluid inflow and outflow conditions. Figures 4 and 5 show the results of the implementation of a two-dimensional flow between two parallel plates. In this case, $Re = 100$ and the velocity in the inlet port is uniform and equal to 1. We can observe, in Fig. 4, the entrance region and the development of the velocity profile. Fig. 5 shows the behavior of the pressure in the center of the plates, $y = 0.5$, as a function of x and compares it with the analytical solution. We observe a good agreement between both solutions.

The ventilated cavity, with no internal obstacle, was then implemented, as depicted in Figs. 6a, 6b and 7, for $Re = 1$, $Re = 100$ and $Re = 500$, respectively. The velocity at the entrance is given by

$$u(y) = -150y^2 + 270y - 120 \qquad \text{for} \qquad 0.8 \leq y \leq 1 \ . \tag{8}$$

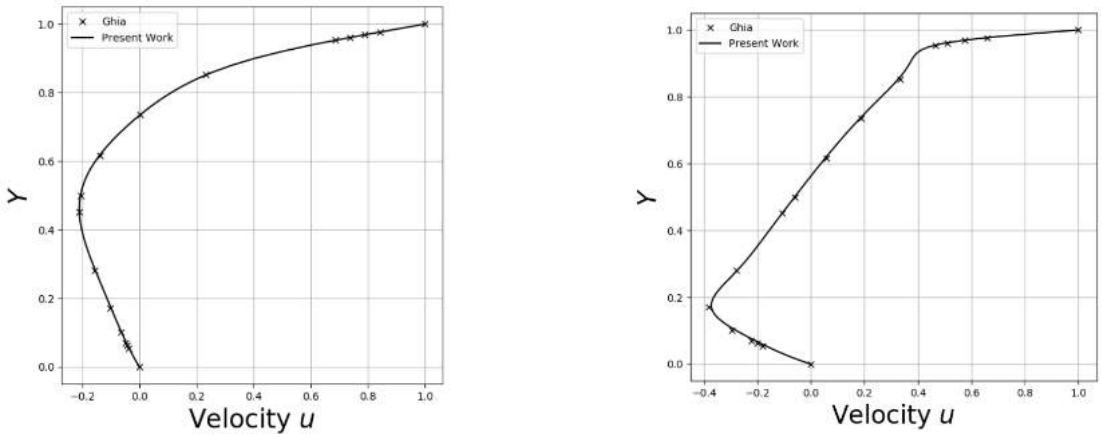

(a) (b)

Figure 3: Comparison between the u-velocity profile for $x = 0.5$ between the present work and the work of Ghia *et al.* (1982), $Re = 100$ (a) and $Re = 1000$ (b).

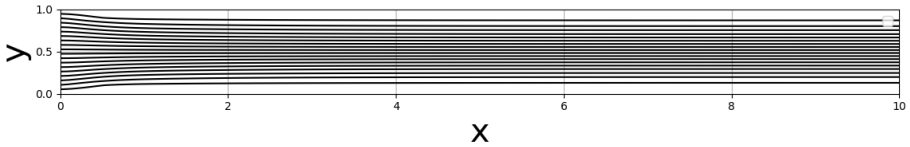

Figure 4: Stream function contour lines for the Poiseuille flow between two parallel plates for $Re = 100$.

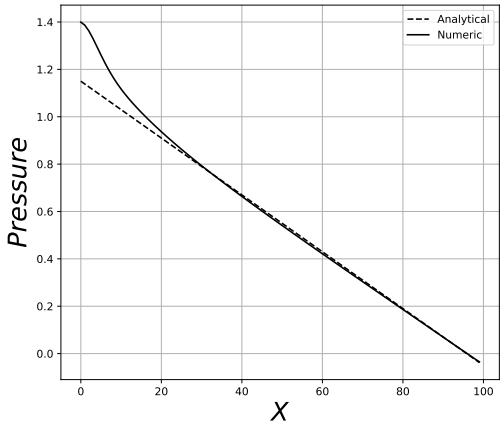

Figure 5: Pressure as a function of distance at $y = 0.5$ for $Re = 100$. The dashed line represents the analytical solution obtained for a parabolic profile.

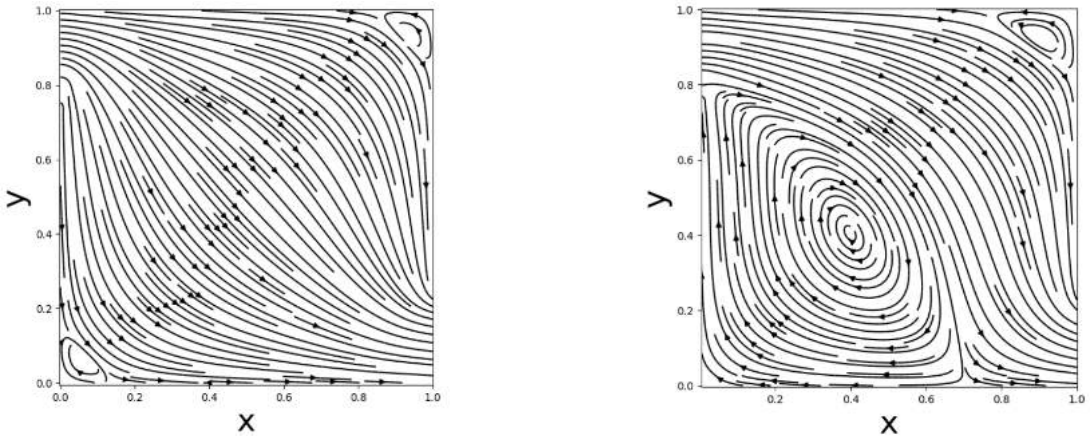

(a) (b)

Figure 6: Streamlines for the flow in a ventilated cavity with $Re = 1$ (a) and $Re = 100$ (b).

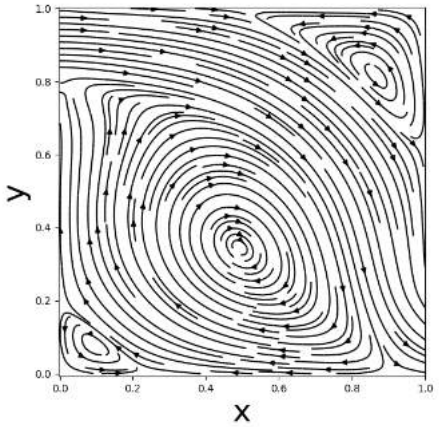

Figure 7: Streamlines for the flow in a ventilated cavity with $Re = 500$.

The results are in qualitative agreement with those obtained by Saeidi and Khodadadi (2006). For these simulations and for all the remaining simulations of this work, $L_{in} = L_{out} = 0.2$ and we use a mesh with 100 points in each direction, resulting in $\Delta x = \Delta y = 0.01$. The time step is 0.005. All results presented here represent the permanent solution, with the final time dependent of the Reynolds number.

4. RESULTS

In Fig. 8a we observe the flow in a ventilated cavity with an internal square obstacle for $Re = 1$. The inlet and the outlet ports are both 0.2 in size and located in the top left and in the bottom right, respectively. The square obstacle obstacle is also 0.2 in size and is located in the center of the cavity. We observe, in this configuration, a very smooth flow around the obstacle. The fluid enters the cavity and contours the obstacles with no recirculation zone, before it leaves the cavity by the outlet port. For this low Reynolds number, the viscosity diffusion dominates the configuration of the flow and the behavior inside the cavity.

A significant different pattern is observed when the Reynolds number is increased to 100, as shown in Fig. 8b. In this configuration, the inertia of the flow entering the cavity is strong enough to keep it in the original direction, leading to the formation of a big vortex region below the inlet port. This vortex occupies approximately $7\,\%$ of the total area of the cavity. In this case we observed no circulation downstream to the obstacle. We can note, in the plot of Fig. 8b, that the flow coming from the entrance contours the obstacle at all sides. This can be important in the situations where the main goal is to obtain an optimum heat exchange between the obstacle and the fluid. If the flow enters the cavity with a low temperature, for example, it will have a large area of contact with the obstacle.

A more complex situation is outlined by Fig. 9, for $Re = 500$. We can observe that in this configuration the obstacle is itself inside a recirculation zone. Now, there is a big vortex that occupies around $50\,\%$ of the total area. Inside this vortex, we can identify two other vortices: one in the bottom left corner of the cavity and one below to the obstacle. The obstacle is not involved, in this case, by the mainstream that comes straight from the entrance. So, if the main goal is to optimize

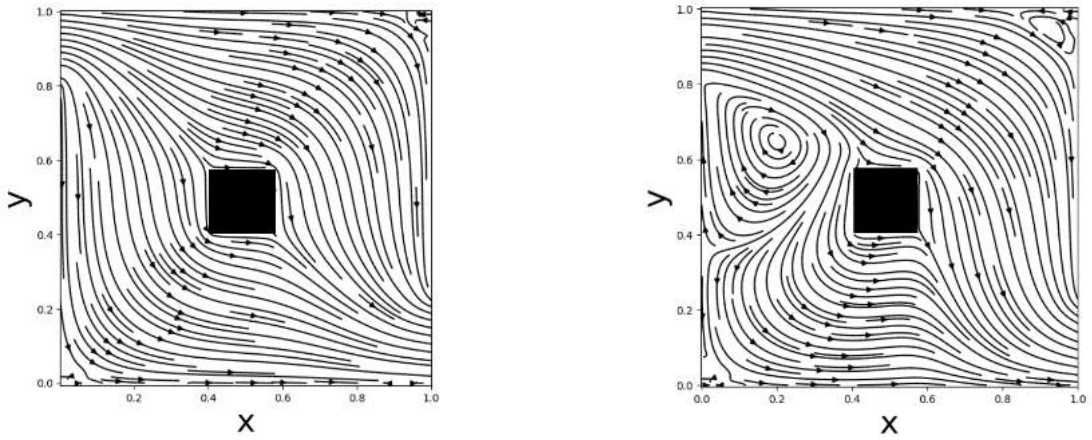

(a) (b)

Figure 8: Streamlines for the flow in a ventilated cavity with one obstacle of size 0.2, $Re = 1$ (a) and $Re = 100$ (b).

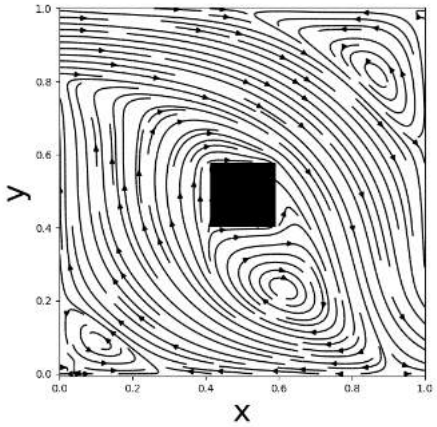

Figure 9: Streamlines for the flow in a ventilated cavity with one obstacle of size 0.2 and $Re = 500$.

the heat exchange between the fluid and the obstacle, this may not be a good configuration.

We make a similar investigation for the flow in a ventilated cavity with a bigger square obstacle, of size 0.5, placed in the center of the cavity. The results are shown in Figs. 10a, 10b and 11, for $Re = 1$, $Re = 100$ and $Re = 500$, respectively. The results show that the bigger obstacle strongly inhibits the formation of vortices inside the cavity. There is only one small vortex for the flow with $Re = 100$, below the entrance port. For $Re = 500$, we can detect one vortex in the entrance, one in top right corner of the cavity and one recirculation zone close to the obstacle. We also observe the main flow contours completely the obstacle, even for $Re = 500$.

The power necessary for the pump to maintain the flow in and out of the cavity is related to the pressure drop between the inlet and the outlet ports. Figure 12 shows the behavior of

$$\Delta p = p_{in} - p_{out} = p(x = 0, y = 0.9) - p(x = 1, y = 0.1)) \tag{9}$$

as a function of the Reynolds number for three configurations: no obstacle, obstacle of size 0.2 and obstacle of size 0.5. The pressure difference is greater for the cavity with the larger obstacle, and smaller for the flow with no obstacle, for every value of Re investigated in this work. This is due to the viscous force acting on the surface of the obstacle. The behavior of the pressure drop, for low Reynolds number, is similar to that observed in the flow between two parallel plates, where $\Delta p \sim Re^{-1}$. For large Re we observe a deviation in this behavior, that might be due to the arising of various and significant recirculation zones. For $Re = 500$, the pressure drop is very similar for the case with no obstacle and for the case with a size 0.2 obstacle. An analysis of Figs. 7 and 9 reveals that the main flow is not significantly affected by the presence of the obstacle for $Re = 500$, since the obstacle is entirely inside a primary recirculation. Thus, the main flow is almost the same, and the pressure drop is quantitatively similar for both situations, a result highlighted by the plot in Fig. 12.

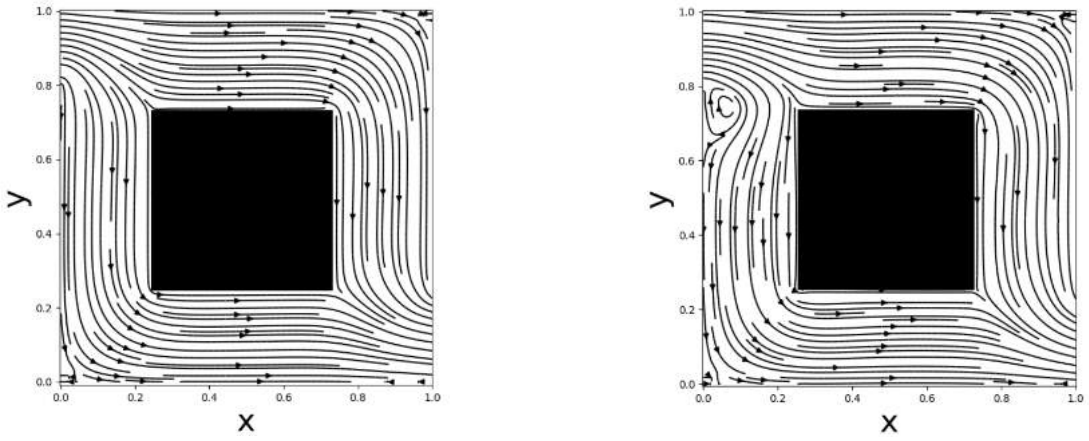

(a) (b)

Figure 10: Streamlines for the flow in a ventilated cavity with one obstacle of size 0.5, $Re = 1$ (a) and $Re = 100$ (b).

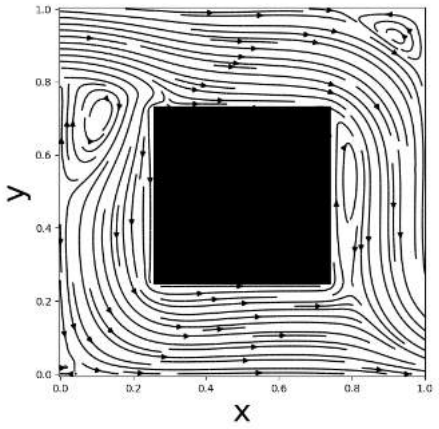

Figure 11: Streamlines for the flow in a ventilated cavity with one obstacle of size 0.5 and $Re = 500$.

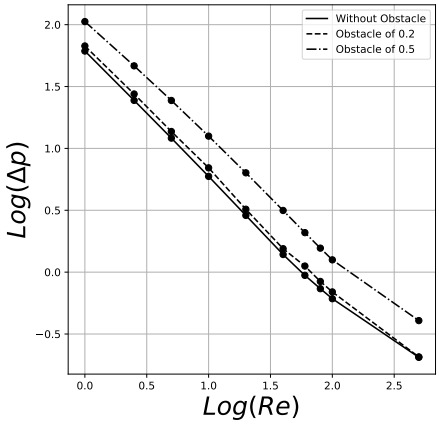

Figure 12: Pressure drop as a function of Re for the ventilated cavity with and without the presence of a central square obstacle.

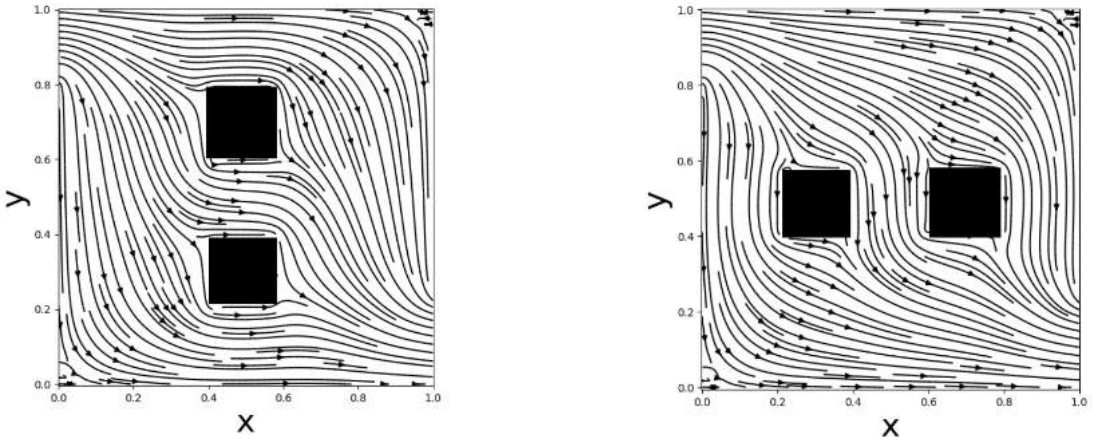

(a) (b)

Figure 13: Visualization of the velocity field for the flow in a ventilated cavity with two obstacles one above the other (a, First Case) and side by side (b, Second Case). Here $Re = 1$.

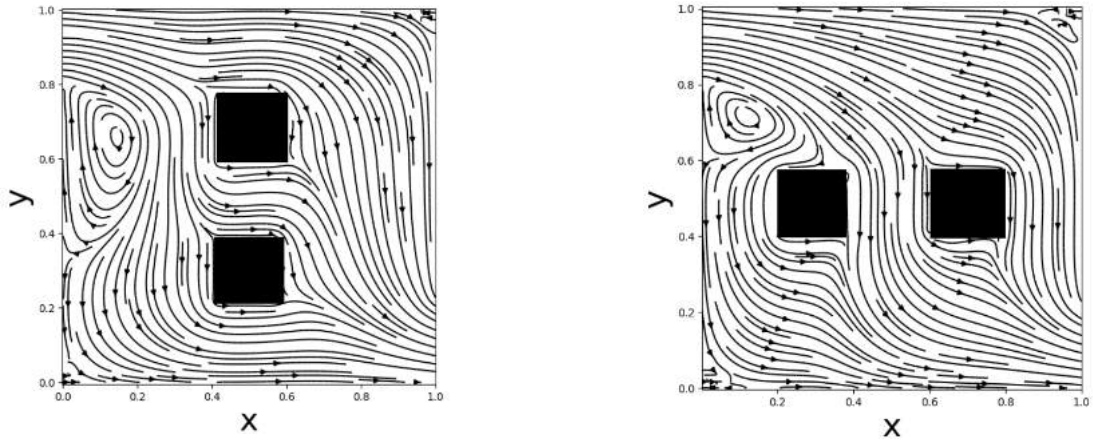

(a) (b)

Figure 14: Visualization of the velocity field for the flow in a ventilated cavity with two obstacles one above the other (a) and side by side (b). Here $Re = 100$.

4.1 Two Obstacles

In this section we investigate the behavior of the flow in a ventilated cavity with two square obstacles of size 0.2 each. Two situations are examined here. The one named *First Case* is characterized by one obstacle placed over the other: the centers of the obstacles are in positions $(x = 0.5, y = 0.3)$ and $(x = 0.5, y = 0.7)$. For the situation designated as *Second Case*, the obstacles are placed side by side, in positions $(x = 0.3, y = 0.5)$ and $(x = 0.7, y = 0.5)$.

The plots in Fig. 13 show the visualization of the flow for a ventilated cavity with two obstacles and $Re = 1$. We observe that the flow is smooth and no remarkable recirculation zone appears in the flow. The momentum diffusion by viscosity dominates the inertia for both configurations and the characteristics of the fluid movement inside the cavity is very similar for them.

The behavior for $Re = 100$ is depicted in Fig. 14. There is now the formation of a vortex in region below the inlet port. The size of this vortex is bigger for the First Case then for the Second Case. However, the remaining structure of the velocity field remains very similar for the two cases, with the obstacle being completely involved by the main flow.

A significant difference between the two cases was found for $Re = 500$, as shown in Fig. 15. For the First Case, a large vortex is formed in the region below the inlet port, occupying an area of about $25\,\%$ of the total cavity area. Also, we note that the main flow contours both obstacles, with a recirculation region downstream to the upper obstacle. For the Second Case we note that the left obstacle in immersed in an even larger vortex, with a total area of $45\,\%$ (including the obstacle) of the cavity. The vortex on the upper right corner is bigger than the one for the First Case, and there are two vortices in the downstream region of the right obstacle.

Despite these qualitatively differences in the analysis of the streamlines in the flow for the First and the Second Cases, no appreciable difference was observed in the pressure drop for the Re investigated in this work, as shown in Fig. 16.

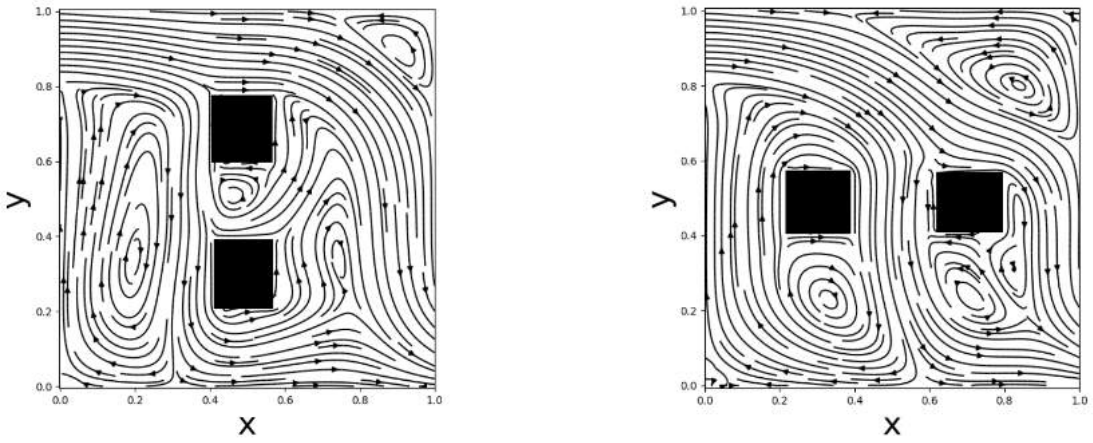

(a) (b)

Figure 15: Visualization of the velocity field for the flow in a ventilated cavity with two obstacles one above the other (a) and side by side (b). Here $Re = 500$.

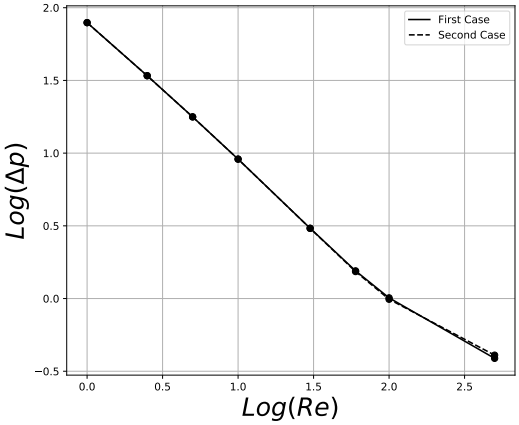

Figure 16: Pressure drop as a function of Re for the ventilated cavity with two obstacles of size 0.2 each. *First Case* corresponds to the obstacles oriented one above the other and *Second Case* refers to the configuration where the obstacles are positioned side by side.

A small difference in Δp is noted only for $Re = 500$. The behavior of Δp is similar to the one of the flow between two parallel plates, with $\Delta p \sim Re^{-1}$. However, the differences in the flow configurations, as discussed in the previous paragraph, can affect drastically the heat exchange between the obstacle and the fluid in the cavity.

5. CONCLUSIONS AND FUTURE WORK

In this paper we investigated the influence of square obstacles on the flow in a ventilated cavity. We observed the behavior of the pressure drop between the inlet and the outlet ports, and also the vortices formation and the change in the flow configurations, with different Re numbers and different obstacle size and positions.

This initial work is part of a project that aims to investigate the possibility of cooling improvement of microelectronic components by the use of complex liquids, such as power-law, viscoelastic and magnetic fluids.

6. REFERENCES

Bell, J.B., Colella, P. and Glaz, H.M., 1989. "A second-order projection method for the incompressible Navier-Stokes equations". *Journal of Computational Physics*, Vol. 85, pp. 257–283.

Botella, O. and Peyret, R., 1998. "Benchmark spectral results on the lid-driven cavity flow". *Computers and Fluids*, Vol. 27, No. 4, pp. 421–433.

Brown, D.L., Cortez, R. and Minion, M.L., 2001. "Accurate projection methods for the incompressible navier-stokes equations". *Journal of Computational Physics*, Vol. 168, pp. 464–499.

Chorin, A.J., 1968. "Numerical solution of the Navier-Stokes equations". *Math Comput*, Vol. 22, pp. 745–762.

Erturk, E., 2009. "Discussions on driven cavity flow". *International Journal for Numerical Methods in Fluids*, Vol. 60, No. 3, pp. 275–294.

Ghia, U., Ghia, K. and Shin, C., 1982. "High-Re solutions for incompressible flow using the Navier-Stokes equations and a multigrid method". *Journal of Computational Physics*, Vol. 48, pp. 387–411.

Kim, J. and Moin, P., 1985. "Application of a fractional-step method to incompressible Navier-Stokes equations". *Journal of Computational Physics*, Vol. 59, pp. 308–323.

Korichi, A. and Oufer, L., 2007. "Heat transfer enhancement in oscillatory flow in channel with periodically upper and lower walls mounted obstacles". *International Journal of Heat and Fluid Flow*, Vol. 28, No. 5, pp. 1003–1012.

Limane, A., Fellouah, H. and Galanis, N., 2015. "Thermo-ventilation study by OpenFOAM of the airflow in a cavity with heated floor". *Building Simulation*, Vol. 8, pp. 271–283.

Madadi, R.R. and Balaji, C., 2008. "Optimization of the location of multiple discrete heat sources in a ventilated cavity using artificial neural networks and micro genetic algorithm". *International Journal of Heat and Mass Transfer*, Vol. 51, No. 9-10, pp. 2299–2312.

Maneshian, B., Javadi, K. and Rahni, M.T., 2019. "Flow control in a cavity with tiny-obstacles on the walls for mixing enhancement part I: Flow physics". *Journal of Applied Fluid Mechanics*, Vol. 12, No. 1, pp. 11–23.

Marchi, C.H., Suero, R. and Araki, L.K., 2009. "The lid-driven square cavity flow: Numerical solution with a 1024 x 1024 grid". *Journal of the Brazilian Society of Mechanical Science and Engineering*, Vol. 31, No. 3, pp. 186–198.

Mushatet, K.S., 2011. "Simulation of laminar natural convection in a cavity with cylindrical obstacles". *Australian Journal of Basic and Applied Sciences*, Vol. 5, No. 6, pp. 636–645.

Saeidi, S.M. and Khodadadi, J.M., 2006. "Forced convection in a square cavity with inlet and outlet ports". *International Journal of Heat and Mass Transfer*, Vol. 49, pp. 1896–1906.

Selimefendigil, F. and Oztop, H., 2014. "Forced convection of ferrofluids in a vented cavity with a rotating cylinder". *International Journal of Thermal Sciences*, Vol. 86, pp. 258–275.

Shankar, P.N. and Deshpande, M.D., 2000. "Fluid Mechanics in the Driven Cavity". *Annual Review of Fluid Mechanics*, Vol. 32, pp. 93–136.

Sourtiji, E., Gorji-Bandpy, M., Ganji, D.D. and Hosseinizadeh, S.F., 2014. "Numerical analysis of mixed convection heat transfer of Al2O3-water nanofluid in a ventilated cavity considering different positions of the outlet port". *Powder Technology*, Vol. 262, pp. 71–81.

Temam, R., 1969. "Sur l'approximation de la solution des equations de Navier-Stokes par la methode des pas fractionnaries II". *Archive for Rational Mechanics and Analysis*, Vol. 33, pp. 377–385.

7. RESPONSIBILITY NOTICE

The authors are the only responsible for the printed material included in this paper.